RSC Advances

PAPER

View Article Online
View Journal | View Issue

Cite this: *RSC Adv.*, 2021, **11**, 20911

A novel ionic AIE smart responsive material with multiple structural transformations†

Zixuan Xu, ‡[a] Linhan Su,‡[b] Xiaofen Chen[a] and Ying Yang *[a]

Received 20th April 2021
Accepted 7th June 2021

DOI: 10.1039/d1ra03090f

rsc.li/rsc-advances

A novel ionic liquid [TPE-Dim-DMe] $(Br)_2$ was successfully synthesiszed. With the change of temperature, quadruple transformations of structure were observed in the [TPE-Dim-DMe] $(Br)_2$ crystal, and it simultaneously displayed mechanochromic phenomena. In addition, its excellent solubility in water makes it a novel bioimaging agent.

Smart luminescent materials, due to tunable luminescence triggered by external stimuli (mechanical force, temperature, pH, solvent polarity *etc.*),[1–5] have widespread applications in mechano-sensors, fluorescent switches, security papers, and data storage.[6–13] However, conventional luminescent materials suffer from aggregation-caused quenching (ACQ), which hinders their development. However, the conventional luminescent materials suffer from aggregation-caused quenching (ACQ), which hinders their development.

In 2001, Tang *et al.*[14] introduced the concept of aggregation induced emission (AIE), which was based on the restriction of intramolecular rotations (RIR). AIE chromophores, such as tetraphenylethene (TPE), exhibit strong fluorescence in solid state or as colloidal aggregates, showing good potential in this field.[15–17]

Some AIEgens exhibit specific mechano-stimuli luminescent response, because grinding and squeezing transform them from a stable structure into other metastable aggregations. However, flexible van der Waals forces allow AIEgens to spontaneously recover to their stable state. Therefore, AIEgens generally show reversible luminescence. This phenomenon is commonly seen during long-term storage or under the influence of external stimulus. Sometimes, the spontaneous transformation is so fast that the emissions of AIEgens become uncontrollable. This severely limits their applications. Hence, restriction of structural transition is the focal point in the development of smart luminescent materials. It is well known that electrostatic forces of attraction are stronger than the van der Waals forces.[18–20]

Therefore, some researches introduced pyridinium salt into TPE with the aim to enhance the structural stability and achieve controllable luminescence.[19] So far, the solid emissions of imidazolyl ionic AIEgens have been seldom examined.

Visual thermosensitive materials have always been in demand for temperature sensing and mapping. Though some polymers, such as PNIPAMs derivatives,[21] display thermo-responsive fluorescence, the response mechanism (the thermal activation of nonradiative deactivation) becomes a disadvantage in terms of a narrow responsive range.[22,23] Thermosensitive materials, with sequential high-resolution temperature response, are seldom reported. Recently, programmed emissions of AIEgens in their solution based on the heating/cooling-driven aggregation transition, were reported.[24] Since the collisions between solvent molecules promote non-radiative decay, the result is a lower emission quantum yield. Meanwhile, due to complexity of the solution system, it is difficult to get an in-depth understanding of the fluorescence response mechanism. In addition, most of AIEgens are endowed with poor sensitivity and regularity to temperature response.[21,25–27] Thus, search for novel thermosensitive materials has become highly challenging. Compared to neutral molecules, organic salts show low melting points, and in fact some of them are ionic liquids (ILs) at room temperature. Hence, organic salts are more likely to undergo phase transformations with broad temperature changes.

Herein, we report the synthese of a novel AIE ionic compounds, [TPE-Dim-DMe] $(Br)_2$, containing TPE and imidazolium bromide. The [TPE-Dim-DMe] $(Br)_2$ crystal showed unique mechanochromic response, wherein the strong blue emissions of the single crystal changed to cyan emissions of the metastable stacks through grinding. The transformation of stacked states is irreversible and even endures thermal annealing and solvent vapor fumigation. Meanwhile, the single crystal of [TPE-Dim-DMe] $(Br)_2$ shows ultra-sensitivity towards temperature. Surprisingly, quadruple transformations were observed in the single crystal with increasing temperature. This variable luminescence was attributed to the synergetic effects between non-radiative transition from molecular thermal

[a]*Key Laboratory of Nonferrous Metals Chemistry and Resources Utilization of Gansu Province, College of Chemistry and Chemical Engineering, Lanzhou University, Lanzhou 730000, Gansu, P. R. China. E-mail: yangying@lzu.edu.cn*

[b]*The 940th Hospital of Joint Logistics Support Force of Chinese PLA, Lanzhou, 730050, Gansu, P. R. China*

† Electronic supplementary information (ESI) available. CCDC 1950798. For ESI and crystallographic data in CIF or other electronic format see DOI: 10.1039/d1ra03090f

‡ Z. X. X and L. H. S contributed equally.

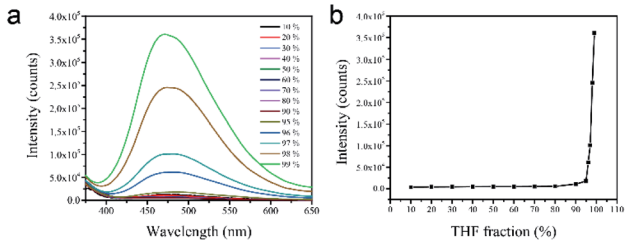

Fig. 1 (a) PL spectra of [TPE-Dim-DMe] $(Br)_2$ in water/THF mixtures with different THF fraction (f_T) concentration: 10^{-4} M; λ_{ex}: 360 nm. (b) Plot of relative emission intensities (I_{max}/I_0) relative to f_T.

motions and structural transformation. In addition, [TPE-Dim-DMe] $(Br)_2$ showed excellent water solubility and low toxicity. It can also be used in bioimaging.

The synthesis of [TPE-Dim-DMe] $(Br)_2$ was carried out by facile three steps, as shown in Scheme S1.† The chemical structure of [TPE-Dim-DMe] $(Br)_2$ was confirmed by ^1H NMR, ^{13}C NMR, HRMS, FT-IR and X-ray single crystal diffraction (Fig. S3–S6† and 2).

The amphiphilic nature enabled [TPE-Dim-DMe] $(Br)_2$ to dissolve in various organic solvents and water. As shown in Fig. 1, [TPE-Dim-DMe] $(Br)_2$ showed relatively weak fluorescence emissions in most organic solvents and water, irrespective of the solvent polarity. Interestingly, [TPE-Dim-DMe] $(Br)_2$ showed a bright blue emission (at ~470 nm) in pure THF. This phenomenon could be attributed to the formation of nano-aggregates. When 5% water was added, the emission decreased remarkably (90% loss). This finding showed that water is an excellent solvent and THF is a poor solvent for the imidazolyl salt. It became evident that [TPE-Dim-DMe] $(Br)_2$ is abnormal AIE molecules. Interestingly, compared to traditional AIEgens, [TPE-Dim-DMe] $(Br)_2$ displayed relatively good solubility in water. Thus, they have great potential for use in bioimaging.

After slow recrystallizing from CH_3CN solution at 25 °C, transparent crystal of [TPE-Dim-DMe] $(Br)_2$ was obtained. As shown in Fig. 2a, XRD classified it to a monoclinic space group $P2_1/c$ [TPE-Dim-DMe] $(Br)_2$ appeared as a highly twisted structure, in which the propeller-like TPE moiety was orthogonally linked with two imidazole rings, forming angles of 85.8° and 82.8° between the planes. Due to the twisted structure, there was no π–π stacking observed between the benzene rings of adjacent AIEgens (Fig. 2b). Meanwhile, the two 1-methyl-imidazole groups partially overlapped with vertical distance of 3.380 Å. Therefore, J-type aggregate was identified for [TPE-Dim-DMe] $(Br)_2$. The monomers were linked within well-organized cells through C–H···π interactions (between the methyl of imidazole and benzene ring of another TPE skeleton) and multiple hydrogen bonds of C–H···O, as well as two kinds of unique bridges: $H_2O\cdots Br^-\cdots H_2O$ and $H_2O\cdots Br^-\cdots H_2O\cdots Br^-$.

The distribution of electron density of the frontier molecular orbitals of [TPE-Dim-DMe] $(Br)_2$ was calculated by density functional theory (DFT) at the B3LYP/6-31+G(d)* level (Fig. 2c and d). The HOMO of [TPE-Dim-DMe] $(Br)_2$ was located on a p-type orbital of bromine (−4.81 eV), whereas the LUMO was distributed mainly on $[TPE\text{-}Dim\text{-}DMe]^{2+}$ (−1.39 eV). This

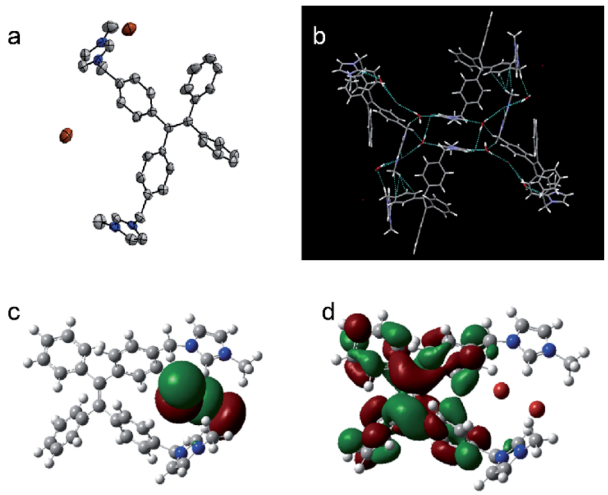

Fig. 2 (a). Single crystal structure and (b). Packing arrangements of [TPE-Dim-DMe] $(Br)_2$, and its (c). HOMO Frontier orbitals and (d). LUMO Frontier orbitals.

indicated that Br^- acted as an electron donor in our study, and $[TPE\text{-}Dim\text{-}DMe]^{2+}$ served as the electron acceptor. A novel charge transfer thus occurred from Br^- to $[TPE\text{-}Dim\text{-}DMe]^{2+}$.[25] This process was distinct from the one present in neutral TPE molecules, wherein the charges were usually transferred from TPE core to the terminal groups.[26,27]

The [TPE-Dim-DMe] $(Br)_2$ crystal showed bright deep-blue fluorescence at 450 nm. Compared with the crystal form, the emission of grinding powder became sky blue in colour and shift to 475 nm (Fig. 3a and b). In the PXRD analyses some diffraction bands for the powder sample were missing, when compared to the crystal form (Fig. 3c). The variation in emissions was due to the structural transformations. Grinding caused the TPE moiety to change from a highly twisted conformation into a flatter structure. Consequently, the well-organized crystal with J-type aggregates underwent

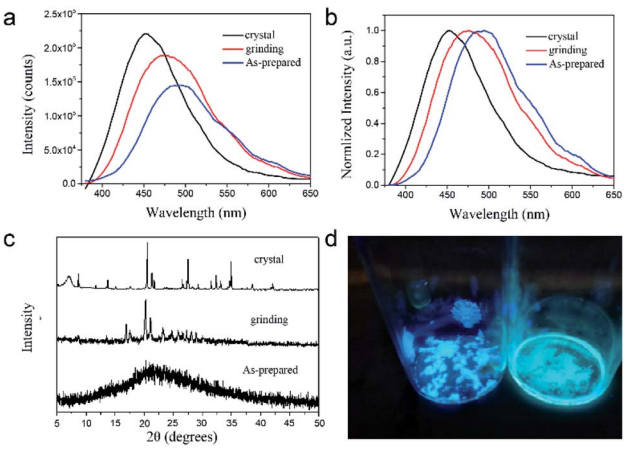

Fig. 3 (a) The solid FL spectra, (b) normalized patterns, and (c) PXRD of $[TPE\text{-}Dim\text{-}DMe]^{2+}[Br]_2{}^2$ in its amorphous powder, crystal and grinding powder. (d) Fluorescent photo of $[TPE\text{-}Dim\text{-}DMe]^{2+}[Br]_2{}^2$ in the amorphous powder and single crystal (illuminating at 365 nm).

transformation into closer aggregates.[28–30] Meanwhile, the multiple hydrogen bonds and C–H···π interactions, which acted as bridges to stabilize the conformation of [TPE-Dim-DMe] $(Br)_2$, were disrupted by mechanical stress to some extent. This caused an increase in disorderliness and rotation of TPE skeleton. The nonradiative decay was therefore enhanced, and the emissions of [TPE-Dim-DMe] $(Br)_2$ powder showed a red shift of 25 nm with weak intensity. The quantum yield Φ_F reduced correspondingly from 57.75% for the crystal form to 46.9% for the powdered sample. In addition, when the solvents evaporated rapidly, a viscous [TPE-Dim-DMe] $(Br)_2$ substance was obtained. The intercalation of residual solvent molecules endowed [TPE-Dim-DMe] $(Br)_2$ with an amorphous structure. The more flexibility in the rotation of TPE skeleton led to cyan emission at ~495 nm with 32.1% quantum yield. Interestingly, the structural transformation from the grinding powder and amorphous state to the single crystal was strongly inhibited, despite vapor fumes and heat. Due to the insensitivity towards environmental interference, [TPE-Dim-DMe] $(Br)_2$ shows promising applications in security papers.

Benefitting from the electrostatic interactions and multiple hydrogen bonds, a relatively stable structure was identified in [TPE-Dim-DMe] $(Br)_2$ crystal. It showed sensitive thermo-response fluorescence over a wide temperature range (Fig. 4a). As the temperature increased from 24 °C to 72 °C, the emissions showed a gradual decline and slight bathochromic shift. The lifetimes diminished simultaneously (Fig. 4b and S10†). Previous reports suggest that high temperature accelerates intramolecular motions or rotations, resulting in decreased energy of excited state by non-radiative transitions.[22,31] Interestingly, the emission intensities depicted a quadruple linear decline over the entire test range (Fig. 4e). The slopes were found to be −161.5 from 24 to 42 °C, −266.43 from 42 to 56 °C, −216.33 from 54 to 60 °C, and-789.71 from 60 to 72 °C. TGA data suggested a negligible mass loss in the tested range. Differential scanning calorimetry (DSC) results also indicated quadruple effect in thermodynamic procedures, consistent with fluorescence transformations in the crystal (Fig. 4d). According to Fig. S10 and Table S3,† the lifetime also exhibited a quadruple linear decline over the entire test range (the slopes were found to be −0.01972 from 24 to 42 °C, −0.0258 from 42 to 56 °C, −0.0206 from 60 to 78 °C.). To further investigate the correlation between emissions and structures, temperature-dependent X-ray diffraction (XRD) analysis of [TPE-Dim-DMe] $(Br)_2$ crystal was performed. Results confirmed that the crystal could endure quadruple structural transformations within their corresponding temperature ranges. At low temperature (from 24 to 42 °C), heat accelerated the vibrations and rotations of covalent bonds and intermolecular forces. The structure hardly showed changes in the monoclinic crystal form. With increase in temperature (from 42 to 48 °C), sharp reflections at 20.2°, 27.3° and 34.6° almost disappeared and a new peak appeared at 24.6°, which indicated the first structural transformation. When the temperature reached 54 °C, the peak at 24.6° disappeared and new reflections appeared at 15.1° and 17.2°, suggesting a second structural transformation. At 60 °C, [TPE-Dim-DMe] $(Br)_2$ showed the third transformation with strong reflections at 20.1°, 22.8°, 24.0°, and 25.4°. Meanwhile, the noise became obvious, because of the increasing disorderliness in the crystal. In addition, the pattern was similar to the XRD pattern of [TPE-Dim-DMe] $(Br)_2$ powder. This suggested that the crystal transforms from the J-type aggregate to disordered closer aggregate. The amazing correlations between quarter structures, decline in emissions, fluorescence lifetimes, and endothermic procedures indicated changes in intermolecular forces and the consequent transformations of crystal phases.

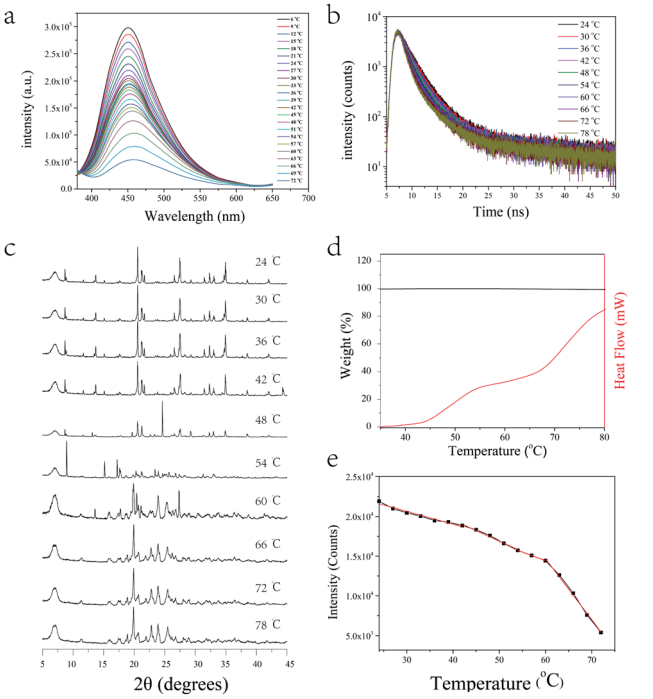

Fig. 4 (a) Temperature-dependent steady-state and (b) transient-state photoluminescence, (c) XRD patterns and (d) TGA of [TPE-Dim-DMe] $(Br)_2$ crystal. (e) Effect of temperature on fluorescent intensity of [TPE-Dim-DMe] $(Br)_2$ crystal.

The aqueous solution of [TPE-Dim-DMe] $(Br)_2$ showed extremely weak fluorescence emissions. In order to further study its aggregation behavior in aqueous medium, a 500 μM aqueous solution of [TPE-Dim-DMe] $(Br)_2$ was used for dynamic light scattering (DLS) testing. Results showed that the average particle size of [TPE-Dim-DMe] $(Br)_2$ in aqueous solution was 30.6 nm, indicating that [TPE-Dim-DMe] $(Br)_2$ had good dispersibility in aqueous solution (Fig. 5). According to the AIE mechanism, [TPE-Dim-DMe] $(Br)_2$ could not form a large supramolecular aggregate in the aqueous medium, which affected its fluorescence emission intensity. It is well-known that cell fluid is a complex water environment. Hence, using [TPE-Dim-DMe] $(Br)_2$ as cell staining agent, it is possible to prevent simultaneously "lighting up" of cells and cell fluids, thereby showing an extremely high signal-to-noise ratio.

In addition, the MTT experiment was conducted to study the cytotoxicity of [TPE-Dim-DMe] $(Br)_2$. As shown in Fig. 6, when the concentration of [TPE-Dim-DMe] $(Br)_2$ was 500 μM, its

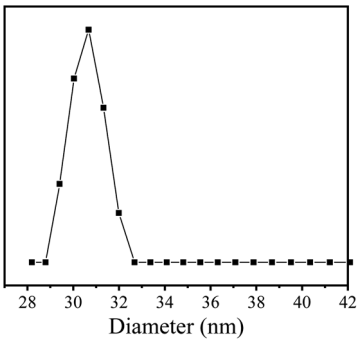

Fig. 5 DLS of [TPE-Dim-DMe] $(Br)_2$ (0.5 mM) in water.

toxicity to HepG2 cells was very low, and the cell survival rate was still above 90%.

$[TPE\text{-}Dim\text{-}DMe]^{2+}$ ions could be electrostatically enriched by phosphate moieties of cell and mitochondrial membrane, which aroused a bright AIE fluorescence inside/on the cell surface. Meanwhile, the excellent water solubility provided [TPE-Dim-DMe] $(Br)_2$ with quenching emissions in the cytoplasm. [TPE-Dim-DMe] $(Br)_2$ could thus be used as an effective bioimaging agent, thereby avoiding the tedious washing procedure to remove the residuals.[32–34] As shown in Fig. 7b and c, clear outlines were seen for cells at 405 (blue) and 488 nm (green) of the double fluorescent channels, after treatment with [TPE-Dim-DMe] $(Br)_2$. Meanwhile, they could be identified against a completely dark background. The high signal-to-noise ratio of cell imaging indicated the superior biological compatibility of [TPE-Dim-DMe] $(Br)_2$.

In summary, a TPE-based ionic compound, [TPE-Dim-DMe] $(Br)_2$ was designed and synthesized. [TPE-Dim-DMe] $(Br)_2$ displayed abnormal AIE characteristics in THF and irreversible mechano-chromic behavior. A thermo-responsive behavior was identified in its crystal form over a wide temperature range. Interestingly, the fluorescence intensities depicted a quadruple linear decline from 24 to 78 °C, which was well consistent with the multi-stage transformations in its fluorescence, TGA, and XRD profiles. The result clearly discloses a close correction among the intermolecular forces, stacking of structure, and

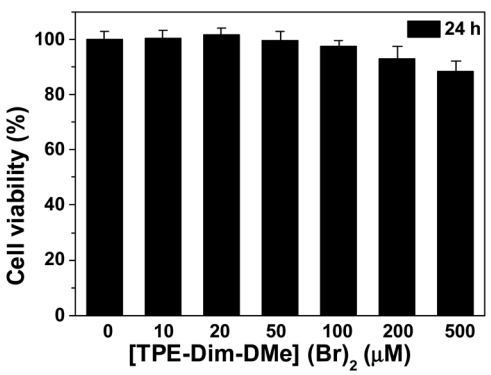

Fig. 6 The cytotoxicity of [TPE-Dim-DMe] $(Br)_2$ in living HepG2 cells for 24 h: 10.0 μM, 20.0 μM, 50.0 μM, 100.0 μM, 200.0 μM and 500.0 μM.

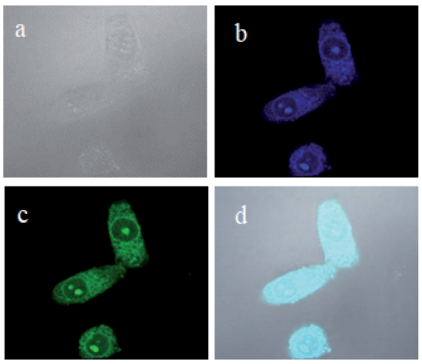

Fig. 7 (a) Bright-field and (b and c) double channel fluorescence and images of HepG2 cells with [TPE-Dim-DMe] $(Br)_2$ (0.50 mM) for 2 min. (d) The merged image of (a–c). Conditions: $\lambda_{ex} = 405$ nm (b) and $\lambda_{ex} = 488$ nm (c).

fluorescence emissions. Moreover, due to its excellent solubility in water and fluorescence features in water, [TPE-Dim-DMe] $(Br)_2$ can be used as wash-free bioimaging agent.

Conflicts of interest

There are no conflicts to declare.

Acknowledgements

The project was financially supported by Major Science and Technology Projects by Gansu Province, China (19ZD2GC001).

Notes and references

1 S. Lee, J. Y. Kim, X. Q. Chen and J. Yoon, *Chem. Commun.*, 2016, **52**, 9178–9196.
2 Z. Chi, X. Zhang, B. Xu, X. Zhou, C. Ma, Y. Zhang, S. Liu and J. Xu, *Chem. Soc. Rev.*, 2012, **41**, 3878–3896.
3 Y. Chen, A. J. H. Spiering, S. Karthikeyan, G. W. M. Peters, E. W. Meijer and R. P. Sijbesma, *Nat. Chem.*, 2012, **4**, 559–562.
4 Y. Zhao, C. Shi, X. Yang, B. Shen, Y. Sun, Y. Chen, X. Xu, H. Sun, K. Yu, B. Yang and Q. Lin, *ACS Nano*, 2016, **10**, 5856–5863.
5 X. Zhang, Z. Chi, Y. Zhang, S. Liu and J. Xu, *J. Mater. Chem. C*, 2013, **1**, 3376–3390.
6 J. Hai, H. Wang, P. P. Sun, T. R. Li, S. Y. Lu, Y. Zhao and B. D. Wang, *ACS Appl. Mater. Interfaces*, 2019, **11**, 44664–44672.
7 X. Zheng, R. Fan, K. Xing, K. Zhu, P. Wang and Y. Yang, *Chem. Eng. J.*, 2020, **380**, 122580.
8 Y. Wang, X. Tan, Y.-M. Zhang, S. Zhu, I. Zhang, B. Yu, K. Wang, B. Yang, M. Li and B. Zou, *J. Am. Chem. Soc.*, 2015, **137**, 931–939.
9 Q. Benito, X. F. Le Goff, S. b. Maron, A. Fargues, A. Garcia, C. Martineau, F. Taulelle, S. Kahlal, T. Gacoin and J.-P. Boilot, *J. Am. Chem. Soc.*, 2014, **136**, 11311–11320.

10 Y. Zhang, Q. Song, K. Wang, W. Mao, F. Cao, J. Sun, L. Zhan, Y. Lv, Y. Ma, B. Zou and C. Zhang, *J. Mater. Chem. C*, 2015, **3**, 3049–3054.
11 H. Li, S. Ye, J. Q. Guo, J. T. Kong, J. Song, Z. H. Kang and J. L. Qu, *J. Mater. Chem. C*, 2019, **7**, 10605–10612.
12 L. Gu, H. F. Shi, L. F. Bian, M. X. Gu, K. Ling, X. Wang, H. L. Ma, S. Z. Cai, W. H. Ning, L. S. Fu, H. Wang, S. Wang, Y. R. Gao, W. Yao, F. W. Huo, Y. T. Tao, Z. F. An, X. G. Liu and W. Huang, *Nat. Photonics*, 2019, **13**, 406–411.
13 Z. F. An, C. Zheng, Y. Tao, R. F. Chen, H. F. Shi, T. Chen, Z. X. Wang, H. H. Li, R. R. Deng, X. G. Liu and W. Huang, *Nat. Mater.*, 2015, **14**, 685–690.
14 J. Luo, Z. Xie, J. W. Lam, L. Cheng, H. Chen, C. Qiu, H. S. Kwok, X. Zhan, Y. Liu, D. Zhu and B. Tang, *Chem. Commun.*, 2001, 1740–1741.
15 X. Cai, N. Xie, Y. Li, J. W. Y. Lam, J. Liu, W. He, J. Wang and B. Z. Tang, *Mater. Horiz.*, 2019, **6**, 2032–2039.
16 H. J. Jin, H. P. Li, Z. Y. Zhu, J. B. Huang, Y. L. Xiao and Y. Yan, *Angew. Chem., Int. Ed.*, 2020, **59**, 10081–10086.
17 L. Zhan, Z. Chen, S. Gong, Y. Xiang, F. Ni, X. Zeng, G. Xie and C. Yang, *Angew. Chem., Int. Ed.*, 2019, **58**, 17651–17655.
18 Z. Wang, Y. Gu, J. Liu, X. Cheng, J. Z. Sun, A. Qin and B. Z. Tang, *J. Mater. Chem. B*, 2018, **6**, 1279–1285.
19 T. Hu, B. Yao, X. Chen, W. Li, Z. Song, A. Qin, J. Z. Sun and B. Z. Tang, *Chem. Commun.*, 2015, **51**, 8849–8852.
20 Y. Wang, G. Zhang, W. Zhang, X. Wang, Y. Wu, T. Liang, X. Hao, H. Fu, Y. Zhao and D. Zhang, *Small*, 2016, **12**, 6554–6561.
21 T. Li, S. He, J. Qu, H. Wu, S. Wu, Z. Zhao, A. Qin, R. Hu and B. Z. Tang, *J. Mater. Chem. C*, 2016, **4**, 2964–2970.
22 M.-M. Xiu, Q. Kang, M.-L. Tao, Y. Chen and Y. Wang, *J. Mater. Chem. C*, 2018, **6**, 5926–5936.
23 Y.-M. Zhang, Y.-F. Li, H. Fang, J.-X. He, B.-R. Yong, H. Yao, T.-B. Wei and Q. Lin, *Soft Matter*, 2018, **14**, 8529–8536.
24 J. Li, Y. Zhang, J. Mei, J. W. Y. Lam, J. Hao and B. Z. Tang, *Chem. –Eur. J.*, 2015, **21**, 907–914.
25 M. K. Salomón-Flores, C. L. Hernández-Juárez, I. J. Bazany-Rodríguez, J. Barroso-Flores, D. Martínez-Otero, R. López-Arteaga, J. Valdés-Martínez and A. Dorazco-González, *Sens. Actuators, B*, 2019, **281**, 462–470.
26 L. Zhu, Y. Shan, R. Wang, D. Liu, C. Zhong, Q. Song and F. Wu, *Chem. –Eur. J.*, 2017, **23**, 4373–4379.
27 T. Jadhav, B. Dhokale, Y. Patil, S. M. Mobin and R. Misra, *J. Phys. Chem. C*, 2016, **120**, 24030–24040.
28 Y. Li, Z. Ma, A. Li, W. Xu, Y. Wang, H. Jiang, K. Wang, Y. Zhao and X. Jia, *ACS Appl. Mater. Interfaces*, 2017, **9**, 8910–8918.
29 Z. Ma, Z. Wang, X. Meng, Z. Ma, Z. Xu, Y. Ma and X. Jia, *Angew. Chem., Int. Ed.*, 2016, **55**, 519–522.
30 J. Xiong, K. Wang, Z. Yao, B. Zou, J. Xu and X.-H. Bu, *ACS Appl. Mater. Interfaces*, 2018, **10**, 5819–5827.
31 Y. Jiang, X. Yang, C. Ma, C. Wang, Y. Chen, F. Dong, B. Yang, K. Yu and Q. Lin, *ACS Appl. Mater. Interfaces*, 2014, **6**, 4650–4657.
32 D. Wang, H. Su, R. T. K. Kwok, X. Hu, H. Zou, Q. Luo, M. M. S. Lee, W. Xu, J. W. Y. Lam and B. Z. Tang, *Chem. Sci.*, 2018, **9**, 3685–3693.
33 R. T. K. Kwok, J. Geng, J. W. Y. Lam, E. Zhao, G. Wang, R. Zhan, B. Liu and B. Z. Tang, *J. Mater. Chem. B*, 2014, **2**, 4134–4141.
34 N. Zhao, M. Li, Y. Yan, J. W. Y. Lam, Y. L. Zhang, Y. S. Zhao, K. S. Wong and B. Z. Tang, *J. Mater. Chem. C*, 2013, **1**, 4640–4646.